



# Plasticity and fracture of AA7075 at elevated strain rates and temperatures

**Conference Paper****Author(s):**

Li, Xueyang; Roth, Christian ; Pandya, Kedar Sanjay ; Karathanasopoulos, Nikolaos; Mohr, Dirk

**Publication date:**

2022

**Permanent link:**

<https://doi.org/10.3929/ethz-b-000592690>

**Rights / license:**

[Creative Commons Attribution 3.0 Unported](#)

**Originally published in:**

IOP Conference Series: Materials Science and Engineering 1238, <https://doi.org/10.1088/1757-899X/1238/1/012006>

# Plasticity and fracture of AA7075 at elevated strain rates and temperatures

X Li, C C Roth, K Pandya, N Karathanasopoulos and D Mohr

Department of Mechanical and Process Engineering, Swiss Federal Institute of Technology (ETH), Zurich, Switzerland

lixue@ethz.ch

**Abstract.** The accurate description of the strain rate and temperature dependent response of Aluminium alloys is a perpetual quest in the hot forming industry. In the present study, uniaxial tension, and notched tension experiments are conducted for an aluminium AA7075-T6 sheet metal at various temperatures and strain rates. The experimental campaign covers strain rates ranging from 0.001/s to 100/s, and temperatures ranging from 20°C to 360°C. We observe low strain rate sensitivity at room temperature, with an increase in strain rate sensitivity as temperature is increased up to 360°C. An YLD2000-3D model is employed to describe the anisotropy of the material. A machine learning based hardening model is employed to capture the complex strain rate and temperature effect on the observed hardening response. Counter-example regularization is utilized to guarantee a convergence in the numeric return-mapping algorithm. Comparing the experimental force-displacement curves with the numerical predictions, the neural network model accurately describes the large deformation response of the material in the post-necking range.

## 1. Introduction

The accurate description of the large deformation response of metals at high strain rates and temperatures is critical in solving industrial problems of hot forming, crash-worthiness, machining, etc. In crash-loading scenarios, aluminum 7xxx series has seen many applications in lightweight structural design, as an alternative to advanced high strength steels [1]. These alloys feature negligible strain rate sensitivity at room temperature, but a high strain rate sensitivity at elevated temperatures [2][3]. Existing models, such as the Johnson-Cook [4] and the Zerilli-Armstrong model [5], prescribe a specific analytical formulation to describe the rate- and temperature dependency. These mechanism-inspired models have been widely adopted over the past decades. Data-driven models based on machine learning algorithms are reported to accurately describe mechanical response of materials at various strain rates and temperatures [6][7][8][9][10]. In the present work, notched tensile experiments are carried out at strain rates from 0.001/s to 100/s in the temperature range between 20°C and 360°C. A neural network based hardening model is proposed, which is trained using a hybrid numerical-experimental approach assisted by counter-example regularization [11]. The model showcases accurate prediction on the force-displacement response, at large deformation in the post-necking regime.



## 2. Experiments at high strain rates and elevated temperatures

### 2.1. Material and Specimen

The AA7075 material is delivered in 2 mm thick sheets and all specimens are extracted using waterjet cutting. Figure 1 shows the two notched tension (NT) geometries considered. The notched tension specimens feature 20 mm wide shoulder section with symmetric circular cut-outs. In this study, a notch radius of  $R = 20$  mm is employed. This reduces the gauge section to a minimum width of 10 mm at the center. The same gauge section is shared by the slow, intermediate and high strain rate tests, with the clamping area adjusted for attaching to different loading systems.

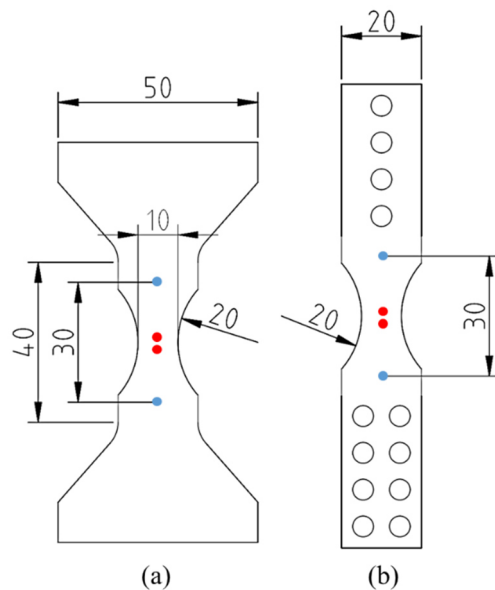


**Figure 1.** Specimen geometries for (a) low, intermediate and (b) high strain rate testing. The blue dots highlight the position of global (30mm) displacement measurements through DIC. The red dots mark the corresponding locations where surface axial strains (1mm) are extracted.

### 2.2. Experimental procedure

**2.2.1. Low strain rate experiments.** The low strain rate experiments are performed on a hydraulic universal testing machine (Instron 8801). Through the build-in control software an actuator speed of 0.4 mm/min is prescribed. This corresponds to an approximate strain rate of 0.001/s. Prior to testing, the specimens are painted with a random black and white speckle pattern for digital image correlation (DIC). The specimens are heated up to the target temperature at a rate of 30K/s using a custom made induction system. This means that for highest temperature of 360°C, the target temperature is reached within 12 seconds. The emissivity of the paint is calibrated to achieve accurate close-loop temperature control using a pyrometer. We verify the homogeneity of the temperature field using an infrared camera (FLIR x6801). A 5MP digital camera (Point Grey GS3-U33-51S5M-C) acquires images for DIC at 1Hz. This achieves a spatial resolution of 25  $\mu\text{m}/\text{pixel}$ .

**2.2.2. Intermediate strain rate experiments.** Experiments at intermediate strain rates are conducted on the same hydraulic testing machine at loading speeds of 40 mm/min and 800 mm/min, corresponding to 100 and 2000 times the speed of the slow tests, respectively. An optical high-speed camera (Photron SA-Z) acquires DIC images at a frequency of 1000 Hz and 8000 Hz. A spatial resolution of 130  $\mu\text{m}/\text{pixel}$  is obtained with this setup. To track the temperature rise caused by plastic dissipation, the infrared camera (FLIR X6801SC) is set up to operate at 2000 Hz. The data and image acquisitions are triggered simultaneously by a rise in the force signal. This allows for a full synchronization between the force and DIC measurements.

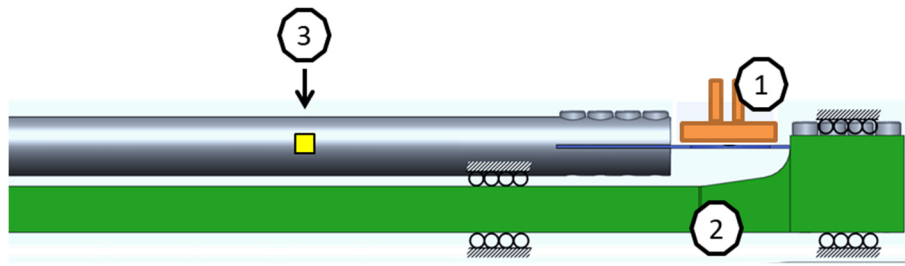


**Figure 2.** Schematic drawing of the high speed – high temperature experiment setup: ① induction heating coil, ② load-inversion device, ③ strain gauge on the output bar.

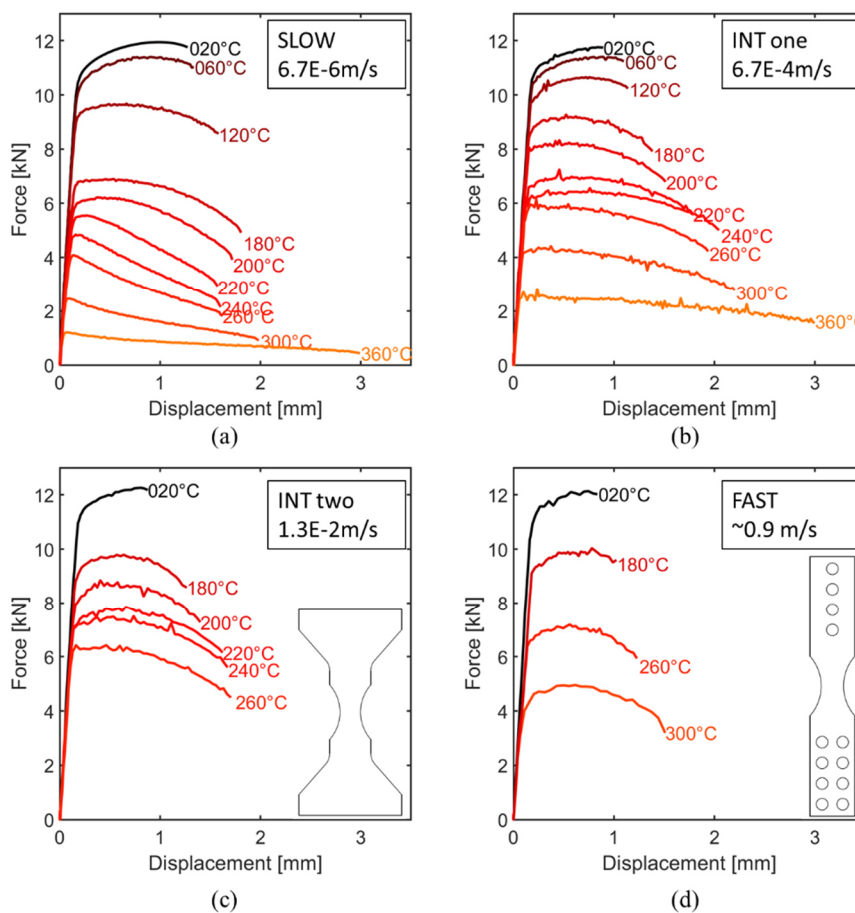


**Figure 3.** Experimentally measured force-displacement curves for NT20 specimens at loading speeds of (a)  $6.7 \times 10^{-6}$  m/s, (b)  $6.7 \times 10^{-4}$  m/s, (c)  $1.3 \times 10^{-2}$  m/s, and (d) 0.9 m/s. All curves are truncated once a crack is visible on the specimen surface.

**2.2.3. High strain rate experiments.** Experiments at high strain rates are carried out on a split Hopkinson pressure bar system. The system includes a 4990 mm long steel striker bar, a 5927 mm long input bar, and a 5951 mm long output bar. All three bars feature an outer diameter of 20 mm. A load inversion device connects the specimen to the input side using eight M5 screws [12]. As illustrated in Figure 2, the custom inductor coil heats up the sheet metal specimen from the top side. The axial force histories

are measured using strain gauges attached on the output bar, located 430 mm from the specimen/output bar interface. To reduce electro-magnetic interference by the inductor upon the strain gauges, the inductor is turned off using a laser signal prior to the striker/input bar impact. The image and data acquisitions are triggered using the rise in the input bar signal. Details of the high speed – high temperature experimental setup are described in [11].

### 2.3. Experimental results

Figure 3 shows the experimentally measured force-displacement curves from the notched tension specimens at various loading speeds and temperatures. The corresponding force maximum extracted from each curve is plotted in figure 4. For all loading speeds, a monotonic and negative effect of temperature on the force-displacement curve is obtained. At room temperature, the effect of strain rate is negligible. Starting from 120°C we observe a significant effect of strain rate on the hardening response of the material. At 300°C, the reaction force increases by 81% when increasing the loading speed by 100 times. This percentage becomes 133% at 360°C, when the hardening response is governed by the viscosity of the material.

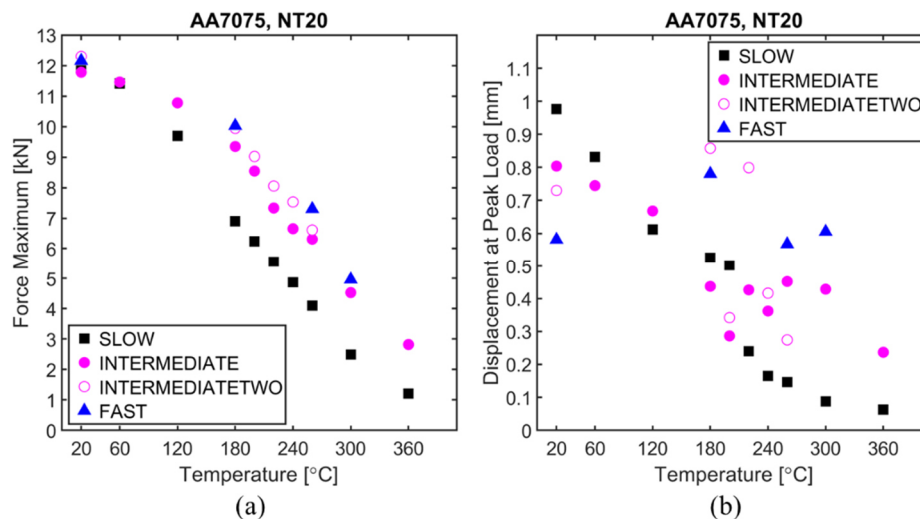


**Figure 4.** (a) The extracted force-maximum as a function of initial temperature for four loading speeds. (b) Displacement at peak load as a function of initial temperature.

## 3. Plasticity models

### 3.1. Model formulation and parameter identification

The material is modeled using an elasto-plastic framework, assuming a constant Young's modulus and Poisson ratio. The yield function consists of an anisotropic equivalent stress  $\bar{\sigma}_{yld2000}$  and the deformation resistance  $k$ ,

$$f[\sigma, k] = \bar{\sigma}_{yld2000} - k = 0. \quad (1)$$

The anisotropy of the material is described using a Yld2000-3D constitutive framework [13], which is an extension to Barlat's Yld2000-2D model [14]. The evolution of equivalent plastic strain is calculated using an associated flow rule. The eight parameters  $\alpha_1 \dots \alpha_8$  describing the yield surface are calibrated from room temperature uniaxial tensile tests along seven different loading orientations from the rolling direction. The formulation of the deformation resistance closely follows [7][11], in which the

deformation resistance is decomposed into a reference mixed Swift-Voce term, multiplied by a neural network term dealing with the effect of strain rate and temperature. Equation 3 details the formulation of the seven parameter hardening function. In the present study, a feed-forward neural network architecture featuring three hidden layers, with ten neurons per layer is selected. Its core concept is subsequent activation of the hidden layers  $H^i$  using the hyperbolic tangent transfer function [15].

$$k[\bar{\varepsilon}_p, \dot{\bar{\varepsilon}}_p, T] = k_{SV}[\bar{\varepsilon}_p] k_{NN}[\bar{\varepsilon}_p, \dot{\bar{\varepsilon}}_p, T] \quad (2)$$

$$k_{SV}[\bar{\varepsilon}_p] = \alpha A(\varepsilon_0 + \bar{\varepsilon}_p)^n + (1 - \alpha)(k_0 + Q(1 - e^{-\beta \bar{\varepsilon}_p})) \quad (3)$$

$$H^0 = [\bar{\varepsilon}_p, \dot{\bar{\varepsilon}}_p, T], H^{n+1} = f(W^n H^n), k_{NN} = f(W^3 H^3) \quad (4)$$

$$f(x) = \tanh(x) \quad (5)$$

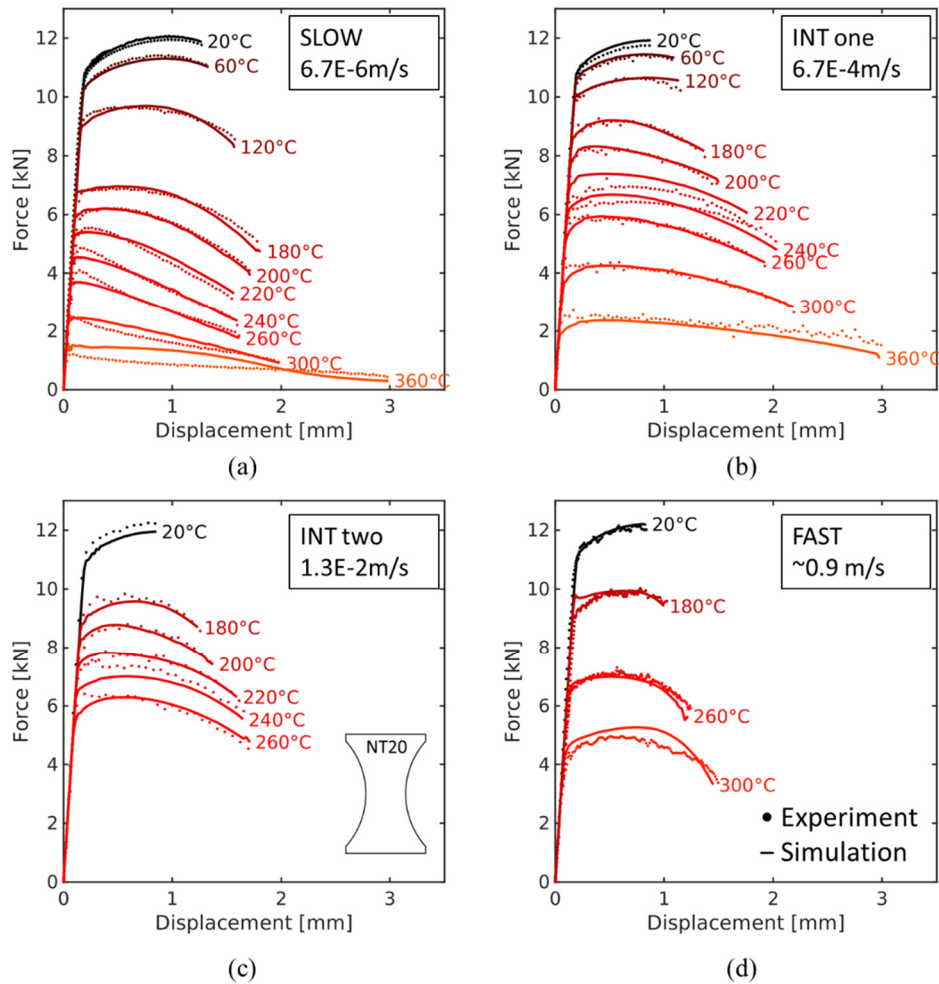


**Figure 5.** Numerically predicted and experimentally measured force-displacement curves at loading speeds of (a)  $6.7 \times 10^{-6}$  m/s, (b)  $6.7 \times 10^{-4}$  m/s, (c)  $1.3 \times 10^{-2}$  m/s, and (d) 0.9 m/s.

The neural network is trained through an inverse-analysis approach in conjunction with back-propagation. To achieve this, the NN is implemented into a user-defined material subroutine in Abaqus/Explicit. To avoid any convergence problems in the numeric return-mapping algorithm due to

negative strain rate sensitivity, counter-example regularization is employed. Details of the parameter identification and the network training process can be found in [11].

### 3.2. Results of numerical modelling

Figure 5 compares the experimentally measured force-displacement curves (solid dots) with the numerical predictions (solid lines) for the NT20 experiments. Overall a good agreement is obtained with the neural network based model, with the largest difference witnessed at room temperature and 0.013m/s. This is due to the slight negative strain rate sensitivity at room temperature from the experiments (Figure 4). At temperatures above 200°C, diffuse necking occurs at very small displacements, followed by a profound post-necking regime before fracture. For all four loading speeds, the neural network model showcases excellent agreement in this range.

## 4. Conclusion

A comprehensive numerical and experimental investigation is performed from quasi-static (0.001/s) to dynamic (~100/s) strain rates on AA7075-T6 sheet metal at temperatures ranging from 20°C to 360°C. The fracture experiments reveal a minimum strain rate sensitivity for AA7075 at room temperature, with an increased strain rate effect as the temperature rises. A machine learning based plasticity model is employed to capture this phenomenon, which decomposes the deformation resistance into a reference mixed Swift-Voce strain hardening term, multiplied with a neural network function that deals with the rate- and temperature dependency. The model is trained using a hybrid numerical-experimental approach, by iteratively running full 3D finite element simulations on NT20 experiments. Counter-example training is employed to circumvent any potential numerical convergence problems in the return-mapping algorithm. The model exhibits good agreement with the experimental force-displacement curves, particularly in the large deformation post-necking regime.

## References

- [1] Fourmeau M, Børvik T, Benallal A and Hopperstad O S 2013 Anisotropic failure modes of high-strength aluminium alloy under various stress states *Int. J. Plast.* **48** 34–53
- [2] Roth C C, Fras T and Mohr D 2020 Dynamic perforation of lightweight armor: Temperature-dependent plasticity and fracture of aluminum 7020-T6 *Mech. Mater.* **149** 103537
- [3] Kabirian F, Khan A S and Pandey A 2014 Negative to positive strain rate sensitivity in 5xxx series aluminum alloys: Experiment and constitutive modeling *Int. J. Plast.* **55** 232–46
- [4] Johnson G R and Cook W H 1985 Fracture characteristics of three metals subjected to various strains, strain rates, temperatures and pressures *Eng. Fract. Mech.* **21** 31–48
- [5] Zerilli F J and Armstrong R W 1987 Dislocation-mechanics-based constitutive relations for material dynamics calculations *J. Appl. Phys.* **61** 1816–25
- [6] Pandya K S, Roth C C and Mohr D 2020 Strain rate and temperature dependent fracture of aluminum alloy 7075: Experiments and neural network modeling *Int. J. Plast.* **135** 102788
- [7] Li X, Roth C C and Mohr D 2019 Machine-learning based temperature- and rate-dependent plasticity model: Application to analysis of fracture experiments on DP steel *Int. J. Plast.* **118** 320–44
- [8] Abueidda D W, Koric S, Sobh N A and Sehitoglu H 2021 Deep learning for plasticity and thermo-viscoplasticity *Int. J. Plast.* **136** 102852
- [9] Jordan B, Gorji M B and Mohr D 2020 Neural network model describing the temperature- And rate-dependent stress-strain response of polypropylene *Int. J. Plast.* **135** 102811
- [10] Shang H, Wu P, Lou Y, Wang J and Chen Q 2022 Machine learning-based modeling of the coupling effect of strain rate and temperature on strain hardening for 5182-O aluminum alloy *J. Mater. Process. Technol.* **302** 117501
- [11] Li X, Roth C C, Bonatti C and Mohr D 2022 Counterexample-trained Neural Network Model of Rate and Temperature Dependent Hardening with Dynamic Strain Aging *Int. J. Plast.* **151** 103218

- [12] Roth C C, Gary G and Mohr D 2015 Compact SHPB System for Intermediate and High Strain Rate Plasticity and Fracture Testing of Sheet Metal *Exp. Mech.* **55** 1803–11
- [13] Dunand M, Maertens A P, Luo M and Mohr D 2012 Experiments and modeling of anisotropic aluminum extrusions under multi-axial loading - Part I: Plasticity *Int. J. Plast.* **36** 34–49
- [14] Barlat F, Brem J C, Yoon J W, Chung K, Dick R E, Lege D J, Pourboghraat F, Choi S-H and Chu E 2003 Plane stress yield function for aluminum alloy sheets — part 1 : theory *Int. J. Plast.* **19** 1297–319
- [15] Bishop 2006 *Pattern Recognition and Machine Learning* Springer